SPACE DEBRIS MITIGATION AND REMEDIATION: PERSPECTIVES OF AFFORDABLE HYBRID PROPULSION IMPLEMENTATIONS

Christian Paravan[(1)], Stefania Carlotti [(1)], Mario A. DiCicco[(1)], Filippo Maggi[(1)], Luciano Galfetti[(2)]

(1) Politecnico di Milano, 34, via LaMasa, 20156, Milan, Italy.
Emails: christian.paravan@polimi.it, steafania.carlotti@polimi.it, marioalberto.dicicco@polimi.it, filippo.maggi@polimi.it, luciano.galfetti@polimi.it

ABSTRACT

In this work, the current development of a vortex flow pancake (VFP) hybrid rocket engine (HRE) is discussed. The early steps for the characterization of the VFP configuration, as well as the whole strategy yielding to its effective and affordable implementation are presented. Thanks to their operating flexibility and their relatively high specific impulse, HREs offer interesting possibilities in in-space propulsion operations. In particular, the VFP configuration features a compact design easing its implementation on different spacecraft platforms. In this perspective, a VFP motor may provide reliable solutions to both space debris mitigation and remediation mission profiles.

1 INTRODUCTION

1.1 Hybrid Rocket Engines: Overview and Perspectives

Hybrid rocket engines (HREs) are thermochemical propulsion systems featuring oxidizer and fuel in different states of matter. In the most commonly implemented configuration, the oxidizer is liquid (or gaseous) and the fuel is solid. In conventional HRE configurations (i.e., cylindrical grains with one or more port perforations) the oxidizer flows over the solid fuel grain generating a boundary layer. After ignition, a diffusion flame is set in this region. The heat transfer from the flame to the condensed phase is mainly due to convection and promotes the fuel gasification [1]. The convective heat transfer is hindered by the mass blowing effect from the condensed phase. As a consequence, the effective heat transfer coefficient is reduced [1]. This, in addition to the diffusion phenomena involved in the combustion process, yields the intrinsic solid fuel regression rate (r_f) limitation characterizing HREs. The main consequence of the low r_f is the relatively low thrust level achievable by HRE. Most of the current research activity on hybrid systems is focused on the study of techniques for r_f enhancement [1][2][3]. The interest for increased r_f and, therefore, high thrust levels, is due to the fact that HREs are mainly seen as competitors of solid rocket motors (SRMs) for launch system applications. This is due to the fact that HREs offer safer manufacturing and transportation with respect to SRMs (thanks to the oxidizer/fuel separation), and an increased operating flexibility (multiple ignitions, thrust throttling). Nevertheless, these attractive features are vanished for space-access applications, where the high burning rates of solid propellant grant high thrust. In this scenario, the main problem is that HREs are taken as candidates for a role that does not fit to their (current) characteristics. On the other hand, HREs offer high performance in terms of I_s. As testified by the data reported in Tab. 1, the vacuum specific impulse ($I_{s,vac}$) of hydroxyl-terminated polybutadiene (HTPB) burning with several oxidizers as liquid oxygen (LOX), H_2O_2 and N_2O are comparable (or higher than) those achieved by ammonium perchlorate (AP)-based solid motors and storable liquid propellants. HREs offer a simplified design over LREs (with consequent implementation cost reduction), thanks to the presence of a single liquid phase reactant. Moreover, lab-scale tests and the so far implemented large scale HREs showed the absence of high-frequency combustion instabilities that may characterize the earlier phases of LREs development. On the other hand, conventional solid fuel grains with cylindrical shapes yields relatively high length-to-diameter ratios (L/D), generally in the range 5 to 10. Depending on the overall grain configuration and ballistics, this may induce oxidizer-to-fuel ratio (O/F) shift during the combustion [4].

In this respect, a non-conventional HRE configuration, the vortex flow pancake (VFP) may yield significant advantages over classical cylindrical grains. In the VFP configuration, an injection ring is placed in between two fuel disks. During the combustion, a vortex flow is set between the two fuel surfaces. Thus, both disks regresses yielding an increase in time of the combustion chamber volume. In this process, the regressing surface area is not affected, the main changed parameter being the distance between the fuel disks. The exhaust gases produced by the combustion flow through the nozzle inlet channel, that is placed in the central port of one of the two disks [1]. This configuration yields a very compact HRE, since high fuel gasification surface area can be achieved by increasing the combustion chamber diameter, and not the engine length (L/D < 1).

Table 1. Vacuum specific impulse ($I_{s,vac}$) of different propellant combinations (NASA CEA code, combustion chamber pressure 2.0 MPa, expansion ratio 70, shifting equilibrium). The first three lines refer to HRE propellant compositions. Note that both N_2O and H_2O_2 may yield exothermic decomposition processes in the presence of a catalyst, and can therefore be employed as monopropellants for RCS.

Fuel	Oxidizer	$I_{s,vac}$, s	O/F	Notes
HTPB	LOX	362	2.40	Cryogenic oxidizer
HTPB	N_2O	320	8.25	Faint O/F influence on $I_{s,vac}$; simplified feed system design
HTPB	H_2O_2	333	6.50	Oxidizer composition 98 wt% H_2O_2, 2 wt% H_2O
N_2H_4	N_2O_4	350	1.40	Hypergolic, widely implemented, highly toxic
HTPB	AP	285	5.7	O/F corresponding to the propellant composition 85 wt% AP + 15 wt% HTPB

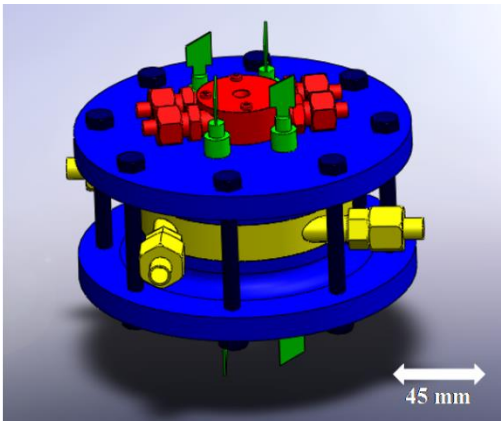

a

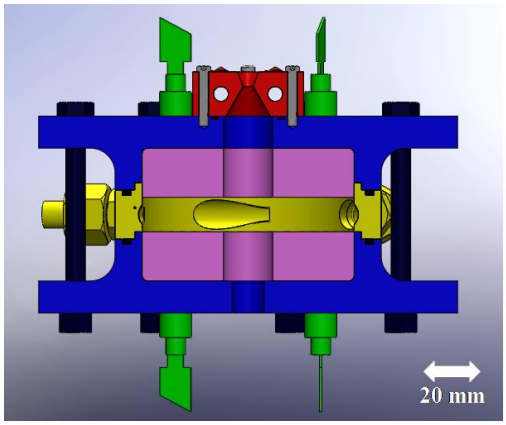

b

Figure 1. SPLab VFP (a) external and (b) cross section views: views: flanges and fuel grain holders (blue), injection ring (yellow), solid fuel grain (violet), water-cooled nozzle (red), and regression rate/fuel grain temperature sensors (green) [7].

Therefore, the VFP configuration grants an easy implementation over different spacecraft platforms. This opens interesting possibilities to the application of such a non-conventional motor geometry in different operating scenarios, as space debris mitigation and remediation.

The VFP motor concept was originally developed and discussed by Caravella et al. [5] and by Gibbon and Haag [6]. The lab-scale VFP motor designed and operating at the Space Propulsion Laboratory (SPLab) of Politecnico di Milano is schematically shown in Fig. 1 [7]. The motor is currently under development and its operating envelope is gradually explored.

1.2 The VFP for Space Debris Mitigation and Remediation

The problem of low earth orbit (LEO) debris that have been accumulating since the beginning of the space-era, requires different strategies for problem mitigation and remediation [8][9][10][11][12]. Debris mitigation strategies based on atmospheric re-entry require footprint minimization. Thus, the precise control of the flight path angle when the spacecraft enters the atmosphere is necessary. From this point of view, chemical propulsion is a good candidate thanks to its higher thrust level compared to other options with higher I_s but incompatible thrust (e.g. electric propulsion). In this respect, the possible uncertainties on satellite residual mass at its end-of-life can impair the precise re-entry trajectory, if the propulsion unit cannot compensate for deviation. In SRMs, the thrust-profile is predetermined and combustion stops/reignitions are not possible, yielding a critical lack of operating flexibility. In a VFP configuration, thrust can be modulated and multiple ignitions can be performed with limited O/F performance shift thanks to the steady burning surface area [6][7]. As a further advantage, with a VFP-based solution, the deorbiting module may act also as a RCS actuator, exploiting main engine firings, or the small thrust produced by decomposition of suitable oxidizers (see

Tab. 1). A similar operating flexibility is shown by LREs. Hypergolic propellants as N_2H_4-N_2O_4 offer multiple ignitions and thrust throttling, though, in this case a more complex design is required due to the doubled feed line. Moreover, for LREs the possible sloshing problems would be doubled too. Considering relatively large objects orbiting in LEO, mitigation operations should focus on the selection and removal of objects of high mass and high collision probability (to reduce the risks of fragmentation in case of impact). A further factor to be considered is the debris altitude. The higher the orbit, the longer the lifetime of the fragments resulting from a collision. In this respect, a joint-program involving SPLab is available in the open-literature [13]. In [13] a VFP configuration is identified as the most suitable for a mitigation mission based on the recovery of multiple debris. In particular, the project focuses on the capture and atmospheric re-entry of Cosmos 3M upper stages. These debris are located at an altitude bands spanning from 650 to 1050 km with orbit inclinations in the range 74 to 83°. A VFP-chaser module is designed to recover these debris. The chaser moves through selected orbits to capture two or three selected debris per mission. After the capture, an atmospheric controlled re-entry is performed. The results discussed in [13], show how a VFP chaser may yield the recovery and disposal of up to three debris per launched platform. In a perspective of cost limitation, the chaser module is sized so that the VEGA launcher (the cheapest vector currently available) could be used for the mission.

2 SPLAB VFP: STRATEGY

SPLab is focused on a strategy aiming at the technical development and implementation of an affordable HRE platform for de-orbiting applications, with tailorable characteristics for both mitigation and remediation scenarios, based on a VFP engine.

In this perspective, strategy summarized by Fig. 2 was developed. Currently, the preliminary characterization phase is performed by internal flow-field analysis (CFD, high-speed visualizations), and firing tests [7]. The flow-field investigation is crucial to evaluate the effective insurgence of a drain type vortex in the combustion chamber, under conditions representing the whole burning envelope of the motor (i.e., from the initial fuel grain thicknesses to the combustion chamber height corresponding to burnout) [7]. The combustion tests are currently performed considering the combustion in gaseous O_2 (GOX) to evaluate the ballistic response of the system under quasi-steady operating conditions without the complication of a liquid oxidizer injection. At the same time, evaluation of oxidizer tanks emptying dynamics and sloshing are ongoing, with a focus on N_2O as case study. The latter is selected as oxidizer considering its attractive features (i.e., simplified feed system thanks to high vapour pressure, and higher long-term stability than H_2O_2) [14].

Representative results on the VFP characterization are discussed in the Sec. 3.1 and in the Sec. 3.2 respectively.

3 SPLAB VFP: NUMERICAL AND EXPERIMENTAL INVESTIGATION

The SPLab VFP is currently realized as a heavy-weight demonstrator for lab-scale activities. The system is designed for a maximum operating combustion chamber pressure (p_c) of 3.0 MPa, while the maximum allowable pressure is 6.0 MPa. The motor is realized in AISI 316 stainless steel. The SPLab VFP test bed enables remote operations during the combustion runs of the engine. A digital flowmeter provides real-time control of the oxidizer mass flow rate ($\dot{m}_{ox}$), while the p_c is monitored by a piezoresistive pressure transducer. Ignition is achieved by a pyrotechnic primer charge.

3.1 VFP Internal Flow-field Numerical Modelling

In this section, results achieved by the CFD analysis of the SPLab VFP internal flow-field are reported. The OpenFOAM® CFD software was used for the simulation. The Reynolds averaged Navier-Stokes (RANS) approach was implemented considering a k-ε model [7]. The ReactingFOAM solver was used with a PISO algorithm [15]. The meshed dominion is shown in Fig. 3. The numerical model motor exhibits differences with respect to the configuration shown in the Fig. 1 for what concern the nozzle geometry. These differences are due to numerical problems for the expanding flow condition. In the numerical model the nozzle shows a peculiar shape with a long throat section, and a divergent of arbitrary diameter. Due to numerical instabilities in the compressible flow solver of the implemented OpenFOAM® version, the minimum section of the modelled nozzle does not correspond to the throat section of the SPLab VFP. Moreover, the diverging part of the nozzle is arbitrarily shaped, to avoid possible numerical instabilities propagation (see [7] for further details). Currently, no combustion process simulation was performed. The motor internal flow-field was evaluated considering the mixing in the combustion chamber of gaseous oxygen (GOX) and butadiene (C_4H_6) vapours. The achieved results are reported in the Figs. 4-6. The internal flow-field of the SPLab VFP shows a vortex structure over both injection and nozzle disk surfaces (see Figs. 4-5).

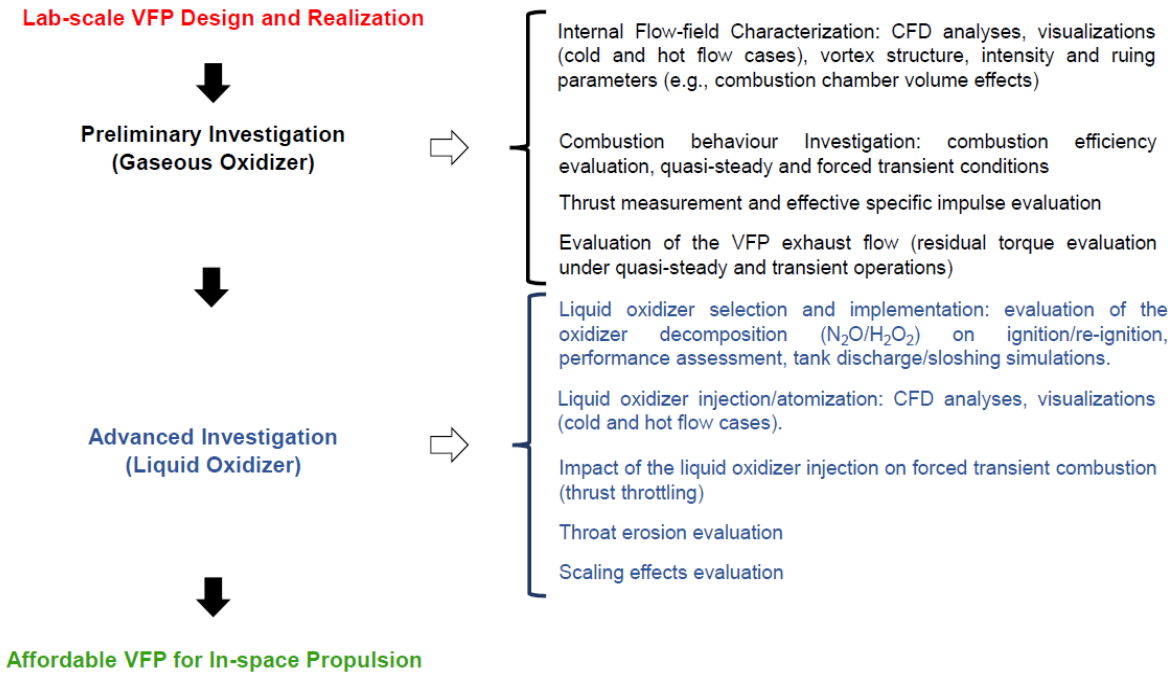

Figure 2. SPLab VFP development flow chart. This work focuses on the preliminary characterization phase, with internal flow-field and combustion behaviour investigation.

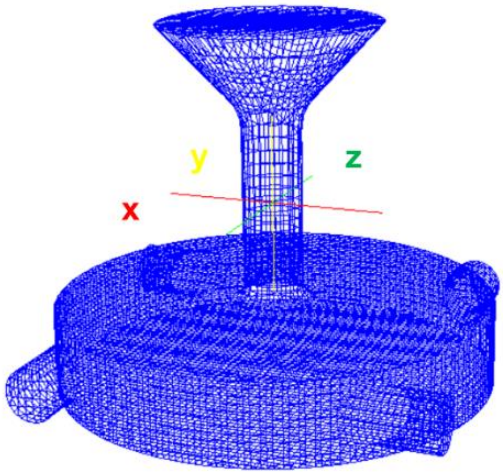

Figure 3. Numerical domain for the internal VFP flow-field simulation.

The oxidizer injection produces the presence of four arms in the vortex structure, that corresponds to the oxidizer injection channels. The relatively high mass flow rate of the oxidizer (with respect to the fuel vapours) highly affects the velocity flow-field, as shown in the Fig. 6. Detailed visualization studies are in progress at the SPLab to validate the achieved numerical results. At the same time, these investigations aim at evaluating the possible vortex combustion effects on the nozzle exhaust flow-field. Residual tangential velocity components may affect the behaviour of the spacecraft platform equipped with a VFP motor. Thus, these effects deserve attention during the engine development and integration phases.

3.2 VFP Combustion Behaviour

The combustion behaviour of the implemented VFP is investigated by quasi-steady burning tests conducted in GOX. Two different fuel formulations were investigated, a thermosetting HTPB binder, and a thermoplastic composition (S40) based on a commercial paraffin wax blended with a reinforcing polymer [16]. The solid fuel regression rate is determined on the base of the weight differences of the solid fuel grains before and after a combustion run. The test duration is defined according to the combustion chamber behaviour in time. The typical $p_c(t)$ trace of a burning test is reported in the Fig. 7, where the main phases characterizing a run are highlighted. Every couple of manufactured fuel grains is usually burnt in multiple runs. At the end of each combustion run, the solid fuel burning is stopped by GOX inlet closure and a nitrogen purge (see Fig. 7). VFP combustion efficiency is evaluated by comparing the experimental characteristic velocity (c^*_{exp}) with the value from the NASA CEA Code [17]. The c^*_{exp} is defined by the overall mass flow rate ($\dot{m}_{ox} + \dot{m}_{fuel}$), the time-averaged combustion chamber pressure ($\overline{p_c(t)}$) and the throat area (A_t), according to the Eq. 1.

$$c^*_{exp} = \frac{\overline{p_c(t)} \cdot A_t}{\dot{m}_{ox} + \dot{m}_{fuel}} \quad (1)$$

The theoretical characteristic velocity (c^*_{th}) for HTPB-GOX is determined by the data reported in [11]. For the S40 formulation, the reinforcing polymer is considered as HTPB, and the paraffin ($C_{50}H_{102}$) heat of formation is taken from [19]. The combustion efficiency is therefore defined as in Eq. 2.

$$\eta_{c*} = \frac{\eta_{c*exp}}{\eta_{c*th}} \quad (2)$$

An overview of the achieved results (r_f and η_{c*}) is reported in the Tab. 2. While the S40 was tested under an oxidizer mass flow rate of 10 g/s, HTPB runs were performed under $\dot{m}_{ox}$ = 8 g/s. For S40, the achieved results show a relatively low combustion efficiency (in the range 0.71 to 0.61) and a decreasing trend of the measured r_f during the different runs of the same test. The first result is probably due to the peculiar characteristics of the S40 fuel, that was tested mainly due to its easy (and fast) manufacturing in the earlier stages of the VFP characterization. This formulation shows a marked viscosity of the melted layer. During the engine inspection in between the runs, unburnt slivers of fuels were found on the combustion chamber and nozzle walls. These slivers are probably detached by the grain surface during the combustion (as testified by the rippled surface of the S40 fuel, see Fig. 8). Solid fuel fragments may have been expelled by the nozzle during the firing, thus justifying the low η_{c*} values. Further investigations are needed to get a better understanding of this phenomenon, since the vortex flow should retain in the combustion chamber the (denser) condensed products, while expelling the (more rarefied) gaseous combustion species. On the other hand, the poor combustion behaviour of the S40 was confirmed also in test performed with conventional geometries [16][20].

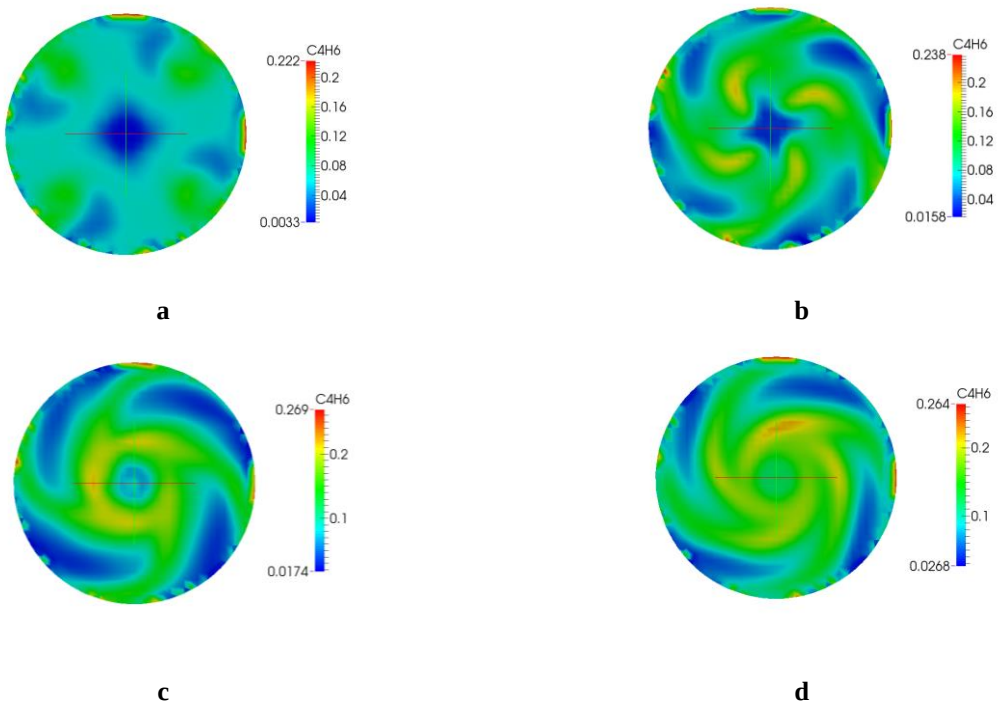

Figure 4. Evolution in time of C_4H_6 mass fraction with oxygen inlet at the igniter-side disk (1 mm over the grain surface): (a) t = 0.00327 s; (b) t = 0.00729 s; (c) t = 0.00939 s; (d) t = 0.01278 s [7].

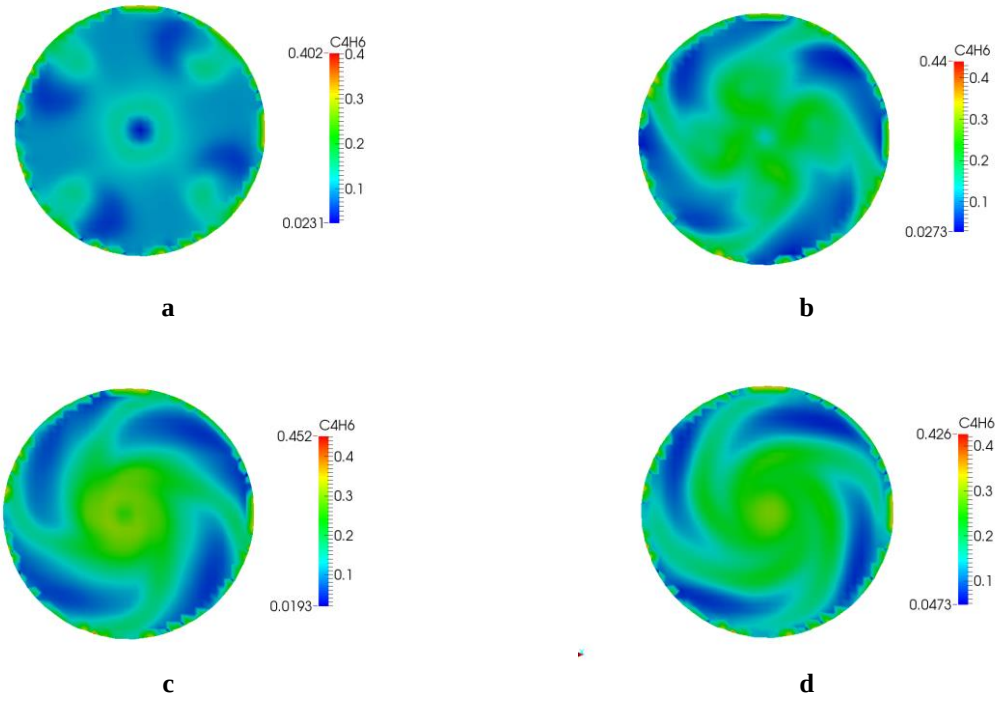

Figure 5. Evolution in time of C_4H_6 mass fraction with oxygen inlet at the nozzle-side disk (1 mm over the grain surface): (a) t = 0.00327 s; (b) t = 0.00729 s; (c) t = 0.00939 s; (d) t = 0.01278 s [7].

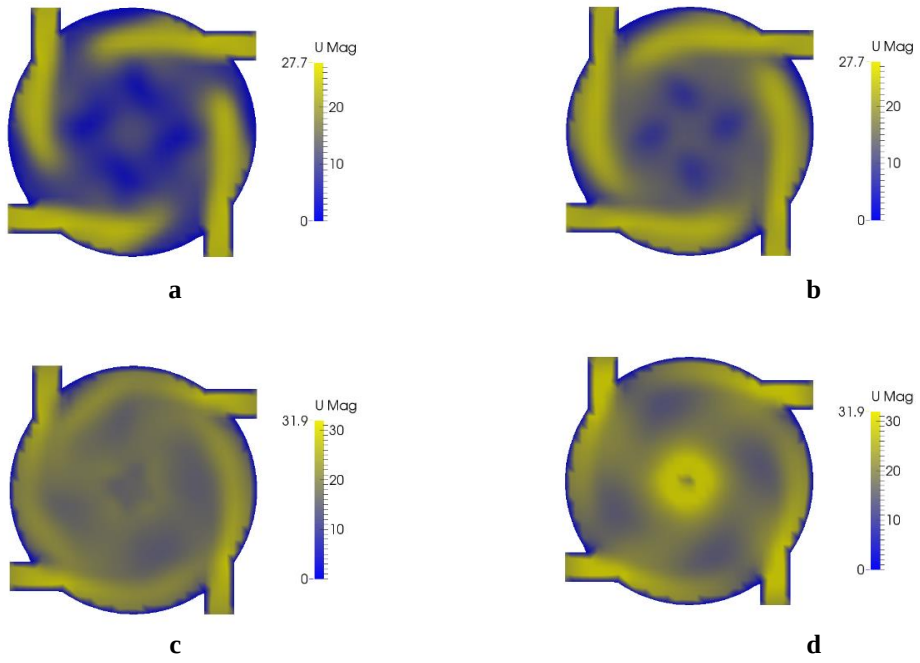

Figure 6. Vortex velocity in the combustion chamber, reference x-z plane in the middle of the chamber: (a) t = 0.00537 s, (b) t = 0.00666 s, (c) t = 0.00793 s, (d) t = 0.00862 s, (e) t = 0.0102 s [7].

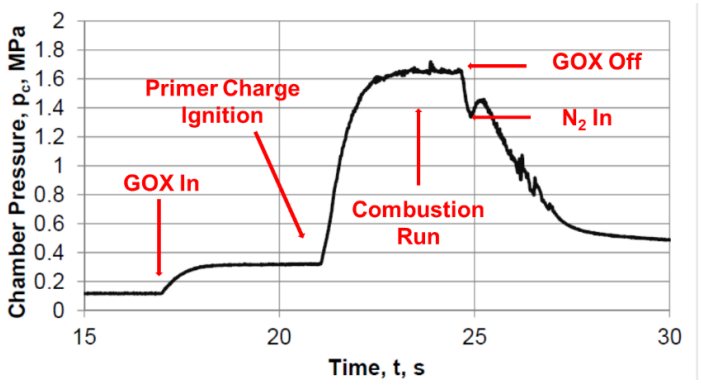

Figure 7. Typical $p_c(t)$ for a VFP combustion run. The beginning of the combustion is defined as the time at which 80% of the maximum measured pressure is achieved. The burning process ends as the nitrogen purge is injected.

Figure 8. S40 Test No. 1, Run No. 1: visualization of the fuel grain surface after the combustion, (a) igniter-disk fuel grain surface, (b) nozzle-disk fuel grain surface. Green arrows show the oxidizer injector positions, red arrows indicate the positions of nozzle and injector rings coupling, the white arrow marks the vortex path

Table 2. SPLab VFP ballistic characterization data for S40 and HTPB fuels burning in GOX ($\dot{m}_{ox}$ of 10 and 8 g/s respectively).

Test No. (Fuel Id.)	Run No.	$\overline{p_c(t)}$, MPa	t_b, s	r_f, mm/s	η_{c*}
1 (S40)	1	1.14	2.82	0.53	0.61
	2	0.51	8.19	0.43	0.68
	3	0.54	5.46	0.38	0.71
2 (S40)	1	0.43	4.01	0.54	NA
3 (S40)	1	0.50	1.50	1.22	NA
	2	0.30	11.6	0.49	NA
1 (HTPB)	1	1.65	4.77	0.50	0.93
2 (HTPB)	1	1.51	4.70	0.54	0.82
3 (HTPB)	1	1.45	3.10	0.66	0.78
	2	1.26	4.21	0.41	0.77
	3	1.06	5.94	0.29	0.77

Tests on the propellant-grade HTPB were performed with a lower $\dot{m}_{ox}$ than the S40 runs. Despite this, the achieved r_f values resulted similar for the two formulations, while the
η_{c*} shows higher values (see Tab. 2). For both S40 and HTPB, the r_f trend is probably due to a change in intensity of the vortex flow as the fuel disks are consumed, and the chamber volume increases [7]. This effect is not discussed in previous open literature works on the VFP configuration [6]. While this phenomenon affects the regression rate behaviour, its influence on the combustion efficiency trend appears limited. Thus, the heat transfer mechanism is strongly affected by the vortex structure. The combustion efficiency is less sensitive to the reduced vorticity since the eventual reduced mixing is compensated by an increase in the residence time of the reacting mixture in the combustion chamber. This phenomenon requires further attention. During the VFP combustion, the r_f behaviour may be compensated by oxidizer mass flow rate throttling, while maintaining relatively high combustion efficiency thanks to the combustion chamber volume increase (i.e., the VFP internal volume acts as a post-combustion chamber enabling complete fuel-oxidizer reaction). On the other hand, the relatively low η_{c*} values achieved during the preliminary investigation are probably due to the limited oxidizer mass flow rates used in the test campaign.

HTPB grain inspections in between the combustion runs showed regular regression surfaces, without fuel slivers accumulation in the combustion chamber or on the nozzle walls (see Fig. 9).

Figure 9. Cross section view of a fired VFP HTPB grain (Test No. 1, nozzle side). The grain profile shows a uniform contour, without anisotropies.

4 CONCLUSIONS AND FUTURE DEVELOPMENTS

This paper discusses the ongoing SPLab activities on the investigation of a lab-scale HRE with a VFP configuration (see Fig. 1). This motor is investigated because of its attractive features that could yield an effective implementation of HRE for in-space applications and, in particular, for mitigation and remediation strategies. The roadmap for the development of a detailed investigation of the VFP configuration is presented, and the current state of the work is discussed.

CFD analyses showed the insurgence of a vortex flow-field under the investigated condition (p_c = 1.0 MPa, $\dot{m}_{ox}$ = 10 g/s), as reported in Figs. 4-6. From the experimental point of view, combustion runs were performed on two different fuel formulations, S40 (a blended formulation of paraffin reinforced by a thermoplastic polymer) and HTPB. The combustion of S40 showed a peculiar behaviour with low combustion efficiencies, probably due to the characteristics of the fuel formulation. The r_f of HTPB-GOX resulted similar to the one of the S40, in spite of a reduced $\dot{m}_{ox}$ (8 g/s vs. 10 g/s). Both S40 and HTPB showed a decreasing regression rate behaviour because of the solid fuel consumption. This effect was not reported in previous VFP investigations available in the open literature [6]. During the tests, multiple ignitions were achieved and no marked combustion anisotropies were identified. The HTPB combustion showed a higher combustion efficiency than the S40. The latter resulted relatively independent from changes in the combustion chamber volume. The achieved results show promising perspectives in the implementation of a hybrid propulsion-based platform enabling efficient and affordable performance for space debris mitigation and remediation strategies. The VFP compact design should enable easy implementation on different systems, while granting adaptive manoeuvring during the deorbiting missions with atmospheric re-entry, thanks to thrust throttling.

Future developments of the work will focus on the roadmap shown in Fig. 2. The next steps of the ongoing preliminary characterization will deal with the cold flow

visualization of the VFP internal vortex structure (for a validation of the achieved CFD results), and on the thrust and specific impulse measurement from the motor.

5 REFERENCES

1. Chiaverini, M.J. (2007). Review of Solid Fuel Regression Rate Behavior in Classical and Non-classical Hybrid Rocket Motors. In: *Fundamentals of Hybrid Rocket Combustion and Propulsion* (Eds. M.J. Chiaverini and K.K. Kuo), Progress in Astronautics and Aeronautics, AIAA, Washington, DC, 2007, Chapter 2, pp. 37–125.
2. Karabeyoglu, M.A., Altman, D., and Cantwell, B.J., (2002) Combustion of Liquefying Hybrid Propellants: Part 1, General Theory. *Journal of Propulsion and Power*, Vol.18, No. 3, pp. 610-620.
3. Karabeyoglu, M.A., and Cantwell, B.J. (2002) Combustion of Liquefying Hybrid Propellants: Part 2, Stability of Liquid Films. *Journal of Propulsion and Power*, Vol.18, No. 3, pp. 621-630.
4. Karabeyoglu, M.A., Toson, E., and Evans, B. (2014) Effects of "O/F Shift" on Combustion Efficiency, AIAA Paper No. 2014-3851.
5. Caravella, J.R., Heister, S.D., and Wernimont, E.J. (1998) Characterization of Fuel Regression in a Radial Flow Hybrid Rocket. *Journal of Propulsion and Power*, Vol.14, No. 1, pp. 51-56.
6. Gibbon, D. M., and Haag, Lin, S., and Kwok, C. K. (2001) Investigation of an Alternative Geometry Hybrid Rocket for Small Spacecraft Orbit Transfer. *DTIC Technical Report*, AD No. 393398, 2001.
7. Paravan, C., Glowacki, J., Carlotti, S., Maggi, F., and Galfetti, L. (2016) Vortex Combustion in a Lab-Scale Hybrid Rocket Motor. *AIAA Paper No. 2016-4562*.
8. Wiedmann, C., Krag, H., Bendisch, J., Sdunnus, H. (2004) Analyzing Costs of Space Debris Mitigation Methods. *Advances in Space Research*, Vol. 34, Nr. 5, pp. 1241-1245.
9. Wormnes, K., Le Letty, R., Summerer, L., Schonenborg, R., Dubuois Matra, O., Luraschi, E., Cropp, A., Krag, H., and Delaval, J. (2013) ESA Technologies for Space Debris Remediation. In: 6th European Conference on Space Debris, 22-25 Apr, Darmstadt, Germany, pp. 1-8.
10. Bonnal, C., Rualt, J.-M., Desjean, M.-C- (2013) Active Debris Removal: Recent Progress and Current trends. Acta Astronautica, Vol 85, pp. 51-60.
11. Lewis, H.G., White, A.E., Crowther, R., Stokes, H. (2011) Synergy of Debris Mitigation and Removal. *International Astronautical Congress*, IAC-11-A6.4.5, Cape Town, South Africa.
12. Liou, J.C. (2011) An Active Debris Removal Parametric Study for LEO Environment Remediation. Orbital Debris Quarterly News, Vol. 47, No. 11, pp. 4-6.
13. Tadini, P., Tancredi, U., Grassi, M., Anselmo, L., Pardini, C., Francesconi, A., Branz, F., Maggi, F., lavagna, M., DeLuca, L.T., Viola, N., Chiesa, S.,Trushlyakov, V.I., Shimada, T. (2014) Cost Estimation of Active Debris Multi-Removal Mission Concept Based on Hybrid Propulsion. *Acta Astronautica*, Vol. 103, pp. 26-35.
14. Heister, S., and Wernimont, E. (2007) Hydrogen Peroxide, Hydroxyl Ammonium Nitrate and Other Storable Oxidizers. In: *Fundamentals of Hybrid Rocket Combustion and Propulsion* (Eds. M.J. Chiaverini and K.K. Kuo), Progress in Astronautics and Aeronautics, AIAA, Washington, DC, 2007, Chapter 11, pp. 457–488.
15. Barton, I. (1998). Comparison of Simple- and PISO-type Algorithms for Transient Flows. *International Journal for Numerical Methods in Fluids*, Vol. 26, No. 4, pp. 459-483.
16. Boiocchi, M., Paravan, C., Dossi, S., Maggi, F., Colombo, G., and Galfetti, L. (2015) Paraffin-based Fuels and Energetic Additives for Hybrid Rocket Propulsion. *AIAA Paper No. 2015-4042*.
17. Gordon, S., and McBride, B.J. (1994) A Computer Program for the Calculation of Complex Chemical Equilibrium Compositions and Applications. *NASA Reference Publication 1311*.
18. Kubota, N. (2015) Propellant and Explosives: Thermochemical Aspects of Combustion – 3rd Edition. Wiley-VCH Verlag GmbH & Co., Weinheim, Germany.
19. Grosse, M. (2009) Effect of a Diaphragm on Performance and Fuel Regression of a Laboratory Scale Hybrid Rocket Motor Using Nitrous Oxide and Paraffin. *AIAA Paper No. 2009-5913*.
20. Ligato, C. (2016) Regression Rate of Paraffin-based Fuels Reinforced by Thermoplastic Polymers. MSc. Dissertation, Politecnico di Milano, Aerospace Science and Technology Department.